SUPPORTING INFORMATION

Dynamic Stabilization of the Ligand-Metal Interface in Atomically Precise Gold Nanoclusters Au$_{68}$ and Au$_{144}$ Protected by *meta*-Mercaptobenzoic Acid

Tiia-Riikka Tero[1,#], Sami Malola[2,#], Benedek Koncz[1,#], Emmi Pohjolainen[2,#], Saara Lautala[2], Satu Mustalahti[1], Perttu Permi[1,3], Gerrit Groenhof[1], Mika Pettersson[1], Hannu Häkkinen[1,2]*

[1] Department of Chemistry, Nanoscience Center, University of Jyväskylä, FI-40014 Jyväskylä, Finland

[2] Department of Physics, Nanoscience Center, University of Jyväskylä, FI-40014 Jyväskylä, Finland

[3] Department of Biology and Environmental Science, Nanoscience Center, University of Jyväskylä, FI-40014 Jyväskylä, Finland

[#] These authors contributed equally
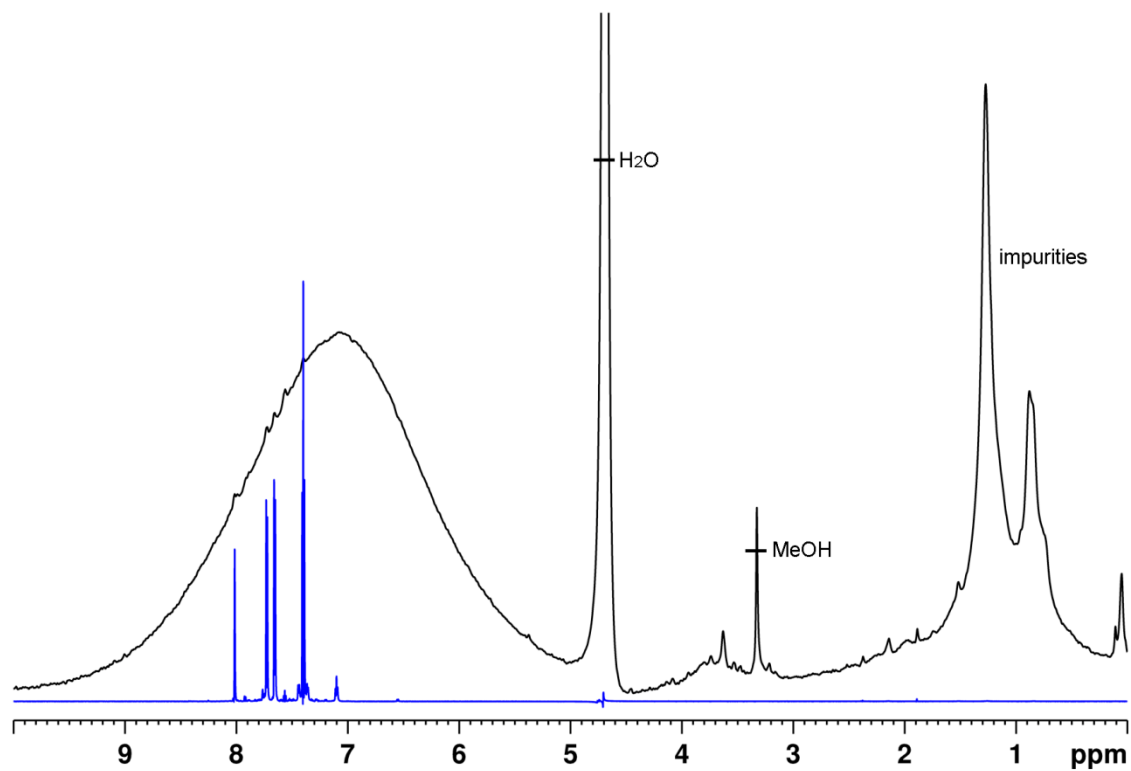
* hannu.j.hakkinen@jyu.fi

A. NMR INVESTIGATIONS

Figure S1. Full ^{1}H NMR spectrum of Au$_{144}$(3-MBA)$_{\sim40}$ (black) and free 3-MBA (blue) in D$_2$O at 800 MHz. The largest resonances of 3-MBA are from a deprotonated form and the smaller ones from protonated and from sulfur bridged dimer.
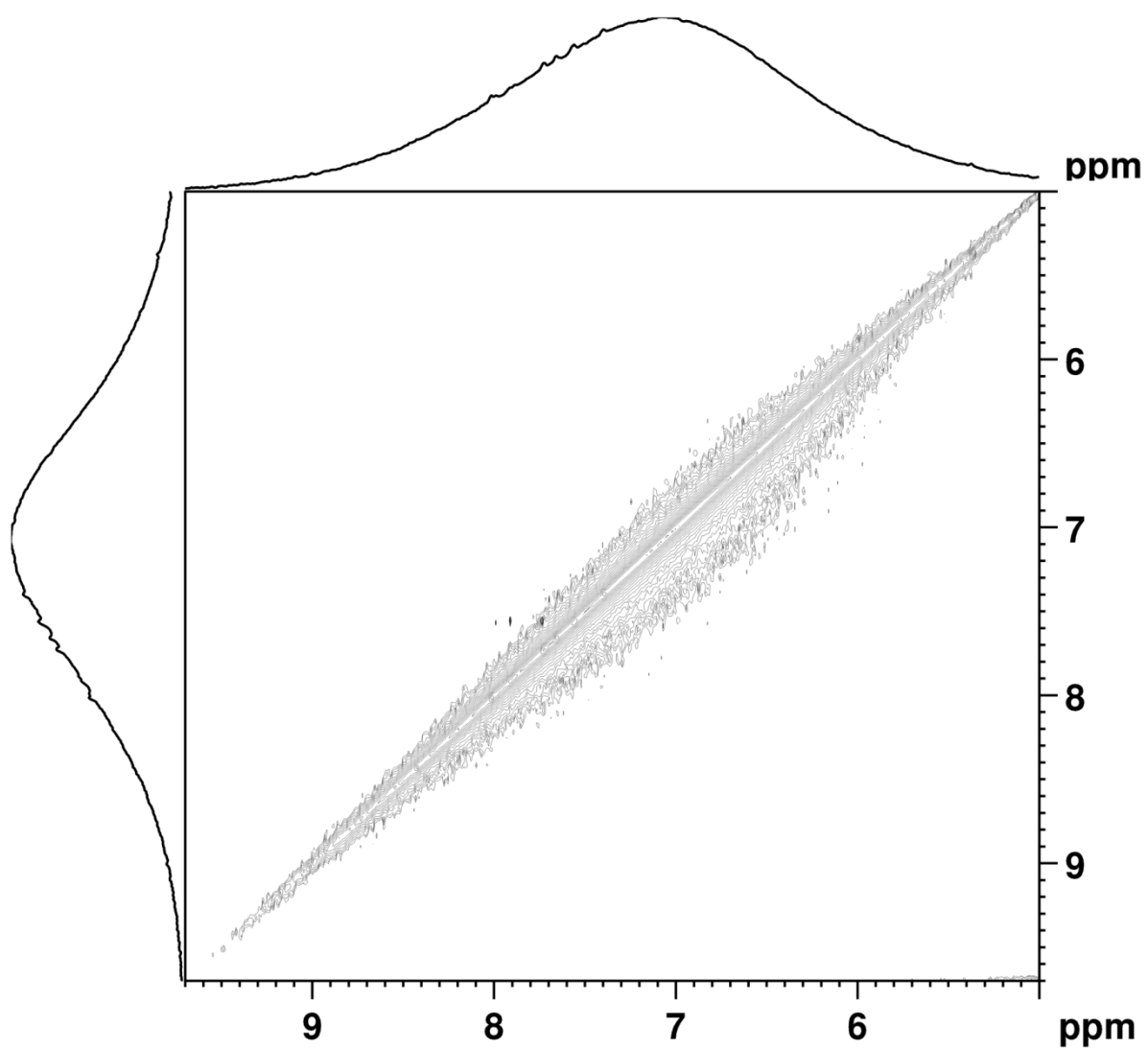
Figure S2. TOCSY spectrum of $Au_{144}(3\text{-MBA})_{\sim 40}$ in D_2O at 800 MHz.
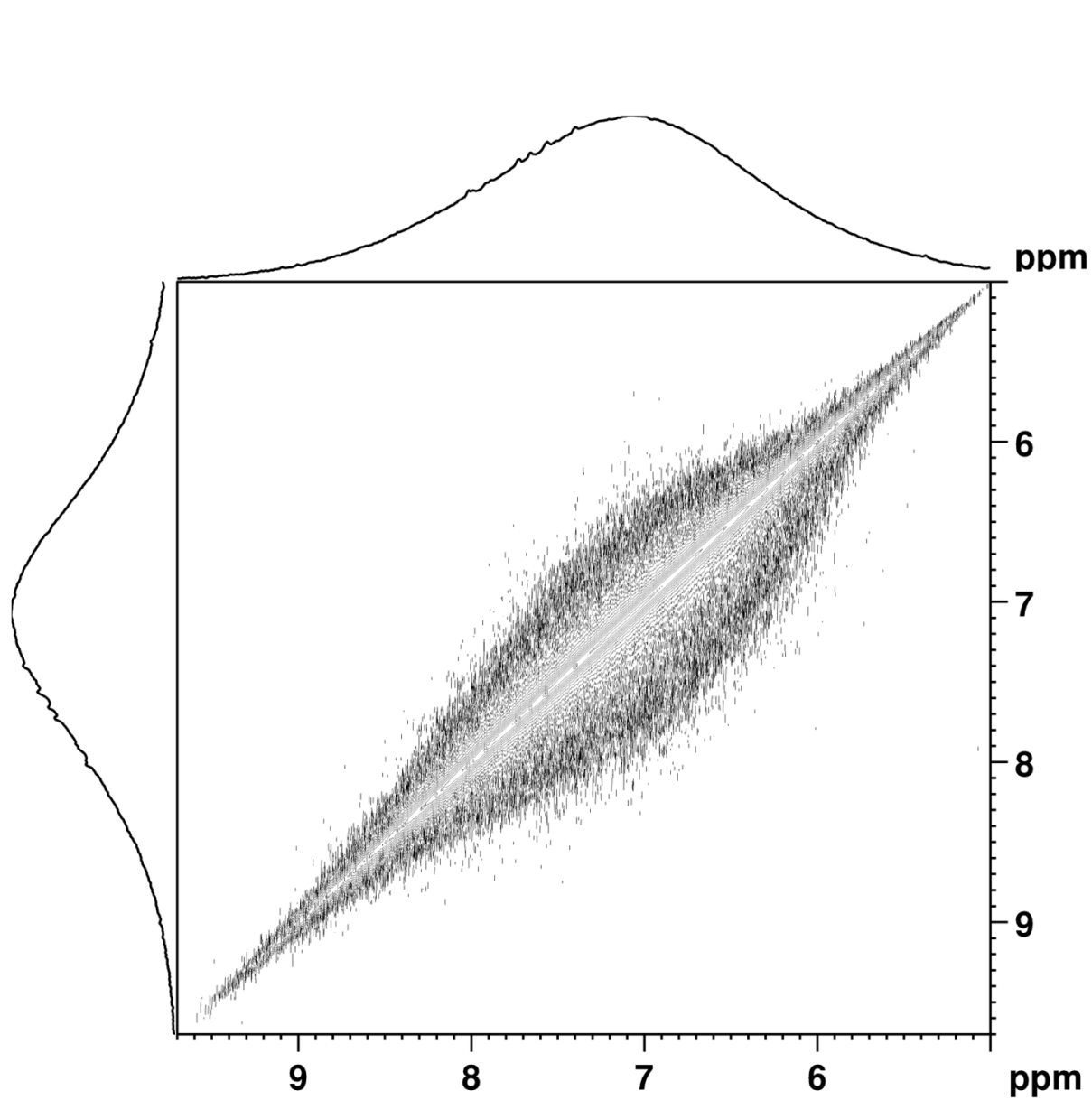
Figure S3. NOESY spectrum of $Au_{144}(3\text{-MBA})_{\sim 40}$ in D_2O at 800 MHz.

Figure S4. Full ^{1}H NMR spectrum of $Au_{68}(3\text{-MBA})_{32}$ in D_2O at 800 MHz. The spectrum shown in blue was measured 7 days after the spectrum shown in black.

Figure S5. TOCSY spectrum of $Au_{68}(3\text{-MBA})_{32}$ in D_2O at 800 MHz. Correlations of five ligands (ligand no 1, 2, 3, 14 and 23, see Table S4) are highlighted with dashed squares as an example.

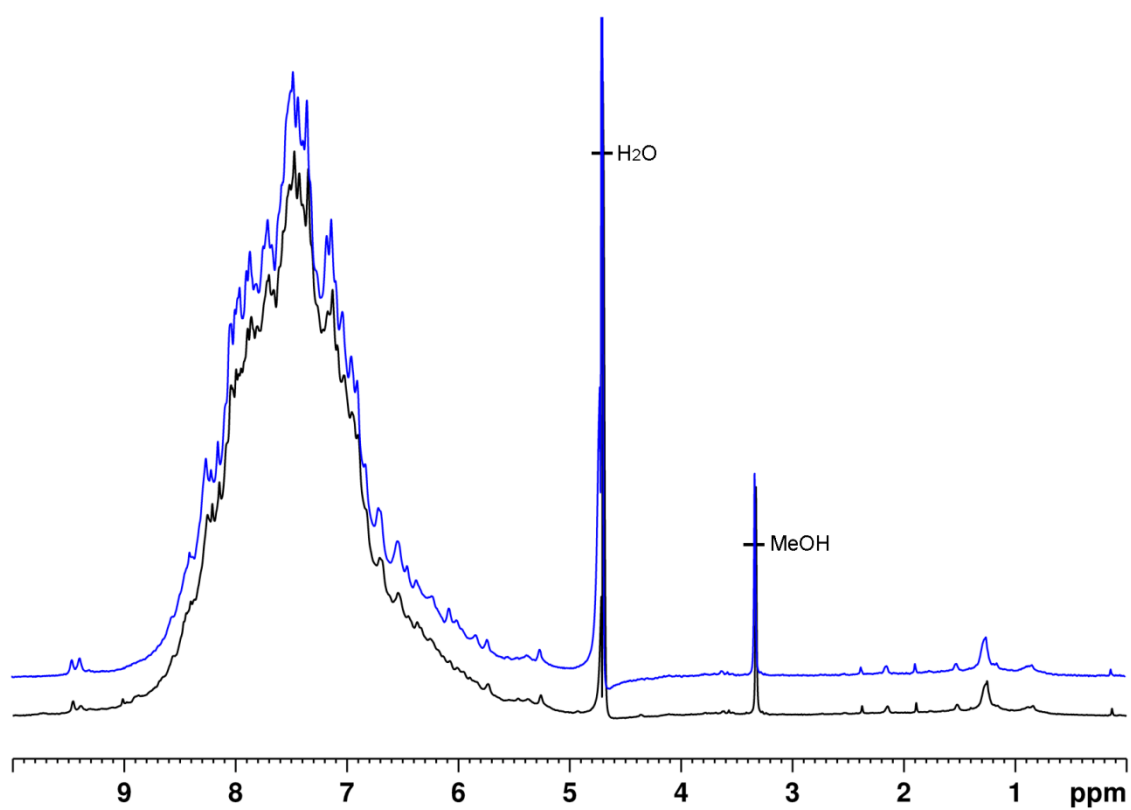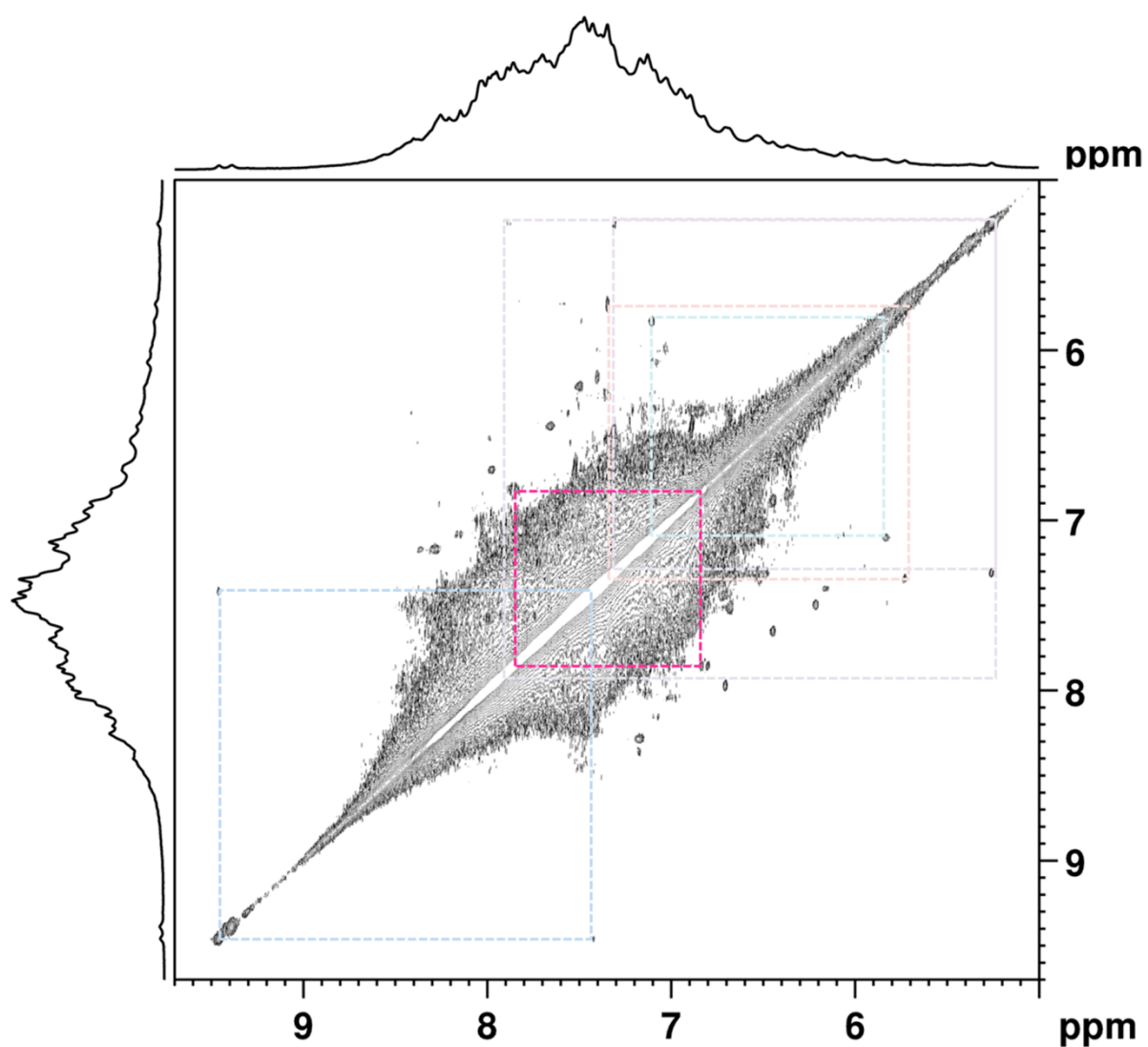**Table S1.** List of resonances from ^{1}H and TOCSY NMR spectra. Resonances are numbered with consecutive numbering and correlating resonances are color coded with different colors.

Res. no	[1]H (ppm)	No of TOCSY correlations	Correlating resonance 1 (ppm)	Correlating resonance 2 (ppm)	NB
1	5.26	2	7.32	7.89	
2	5.38	0			
3	5.73	1	7.35		
4	5.83	1	7.11		
5	5.90	0			
6	5.96	0			
7	6.01	0			
8	6.08	1	7.09		
9	6.17	1	7.4		
10	6.21	1	7.49		
11	6.25	1	7.35		Weak
12	6.33	0			
13	6.37	2	6.85	6.67	
14	6.42	0			
15	6.45	2	6.89	7.66	
16	6.54	2	7.04	7.31	Two signals overlapping?
17	6.63	0			
18	6.67	1	6.37		
19	6.68	2	7.52	7.13	
20	6.70	1	6.93		
21	6.71	1	7.97		
22	6.72	1	7.45		
23	6.81	1	7.86		Doublet with 6.83 ppm
24	6.82	1	6.96		
23	6.83	1	7.84		Doublet with 6.81 ppm
25	6.85	1	6.37		
26	6.89	1	6.45		
27	6.90	1	7.48		Doublet
28	6.91	1	7.64		
29	6.93	1	6.7		
30	6.96	1	6.82		
31	6.99	1	8.04		Weak
32	7.02	1	6.52		
33	7.04	1	6.54		
34	7.07	1	8.15		
35	7.09	1	6.08		Doublet
36	7.11	1	5.83		
37	7.12	2	7.81	7.58	Doublet
38	7.13	1	6.68		
39	7.17	2	8.28	8.37	
40	7.21	0			

41	7.25	1	7.72		
42	7.27	0			
43	7.31	1	6.54		
44	7.32	2	5.26		
45	7.35	2	5.73	6.25 (d)	
46	7.40	1	6.17		
47	7.43	1	9.46		
48	7.45	1	6.72		
49	7.47	0			
50	7.48	1	6.9		Doublet
51	7.49	1	6.21		
52	7.52	1	6.68		
53	7.54	0			
54	7.57	2	7.99	7.92	
55	7.58	1	7.12		
56	7.64	1	6.91		Doublet
57	7.66	1	6.45		
58	7.70	0			
59	7.72	1	7.25		
60	7.75	0			
61	7.81	1	7.12		Doublet
62	7.84	1	6.81		Doublet with 7.88 ppm
62	7.88	1	6.81	6.83	Doublet with 7.84 ppm
63	7.89	1	5.26		Doublet
64	7.92	1	7.57		Doublet
65	7.95	0			
66	7.97	1	6.71		
67	7.99	1	7.57		
68	8.03	0			
69	8.04	1	6.99		Doublet, weak
70	8.09	0			
71	8.15	1	7.07		Doublet, weak
72	8.21	0			
73	8.25	0			
74	8.28	1	7.17		
75	8.37	1	7.17		
76	8.40	1	6.54		Doublet, weak
77	8.44	0			
78	8.57	0			
79	9.39	0			
80	9.46	1	7.43		

^{1}H and TOCSY NMR spectra showed 80 resonances, but since the signals are very close to one another and most likely also overlapping the actual number of resonances is much higher. Heteronuclear single quantum correlation (HSQC) experiment correlates a proton with its directly bonded carbon. ^{13}C-HSQC spectrum of $Au_{68}(3\text{-MBA})_{32}$ displayed superior

chemical shift dispersion with respect to the TOCSY spectrum (Table S2). Several overlapping ^{1}H resonances and cross peaks in TOCSY were distinguishable in ^{13}C-HSQC spectrum owing to their differing ^{13}C ppm frequencies.
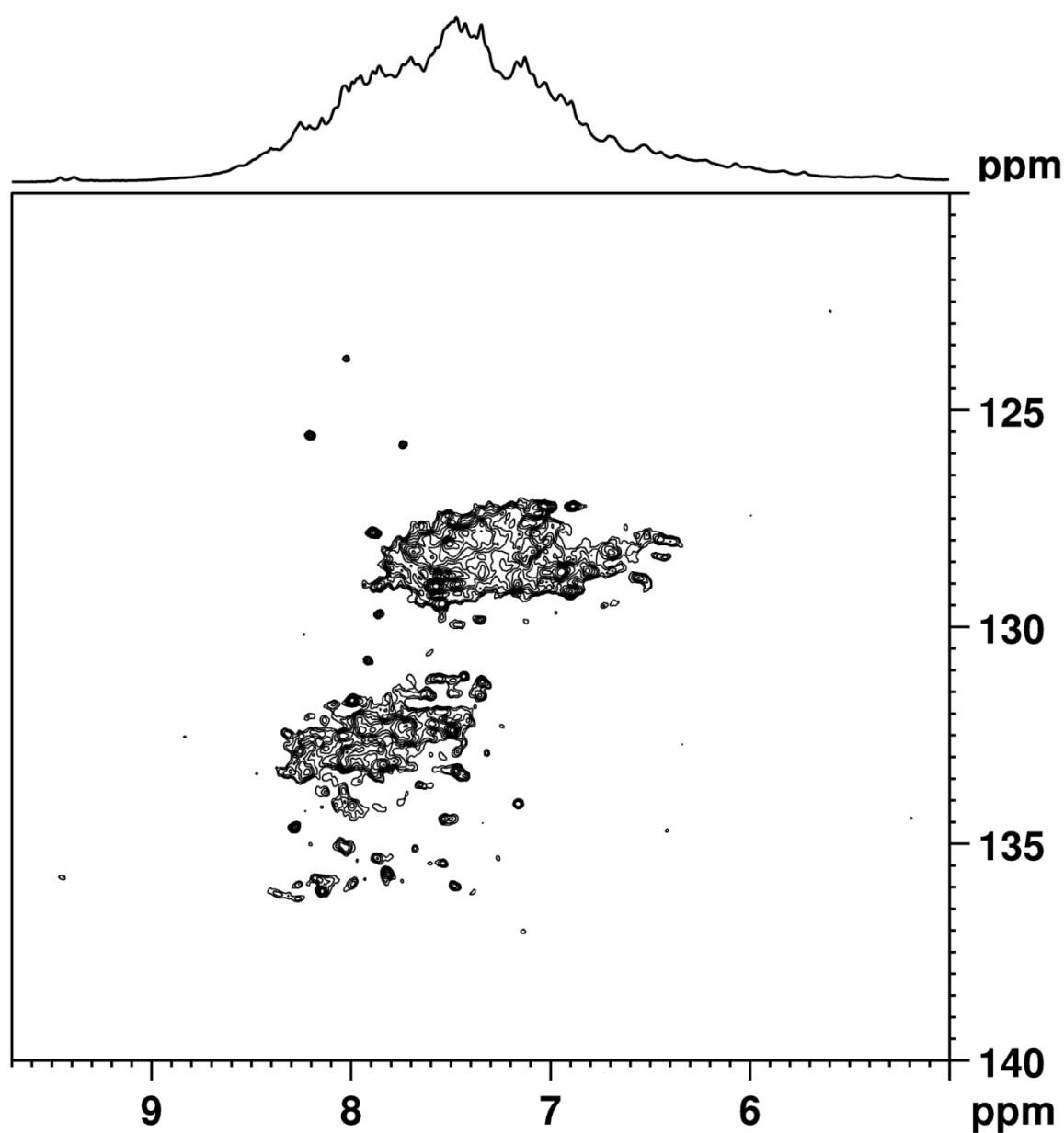

Figure S6. ^{13}C-HSQC spectrum of $Au_{68}(3\text{-MBA})_{32}$ in D_2O at 800 MHz.

Table S2. List of resonances from ^{1}H, TOCSY and ^{13}C-HSQC NMR spectra with ^{1}H-^{13}C correlations. Signals with consecutive numbering were observed in ^{1}H and TOCSY, signals without number were observed from HSQC.

Correlation no in TOCSY	^{1}H (ppm)	^{13}C (ppm)	NB
	5.19	134.4	
1	5.26	128.2	
2	5.38		
	5.60	122.7	
3	5.73	128.4	
4	5.83		
5	5.90	133.0	Weak
6	5.96	127.4	Weak
7	6.01	127.4	
8	6.08	128.7	
9	6.17		
10	6.21	129.0	
11	6.25		
12	6.33	132.7	
13	6.37	128.1	
14	6.42	134.7	
	6.44	128.4	
15	6.45	128.0	
	6.48	136.5	
	6.52	127.9	
16	6.54	128.9	
17	6.63	127.7	
18	6.67	128.3/128.7	
19	6.68	128.3/128.7	
	6.68	129.5	
20	6.70	128.3/128.7	
21	6.71	129.2	
22	6.72	129.5	
23	6.81	128.7	
24	6.82	128.8	
23	6.83		
25	6.85		
26	6.89	127.2	
27	6.90	129.2	
28	6.91		
29	6.93	128.8	
30	6.96	128.8	
	6.97	129.7	Weak
31	6.99		
32	7.02	128.1	

	7.03	127.2
33	7.04	128.8
34	7.07	127.6
35	7.09	129.1
36	7.11	127.7-128.5
37	7.12	127.7-128.6
38	7.13	127.7-128.7
	7.14	137.0
	7.16	134.1
39	7.17	129.1
40	7.21	
41	7.25	132.3
42	7.27	135.3
43	7.31	128.0
44	7.32	132.9
	7.34	131.3
45	7.35	128.8
	7.36	129.9
	7.36	131.6
46	7.40	136.1
	7.42	132.2
47	7.43	127.8
	7.43	131.2
48	7.45	129.1
49	7.47	133.3
50	7.48	136.0
51	7.49	132.4
	7.49	131.2
52	7.52	128.1
53	7.54	134.5
	7.54	135.5
	7.54	129.5
	7.55	132.0
	7.56	131.2
54	7.57	129.1
55	7.58	132.2
	7.60	133.7
	7.61	131.6
56	7.64	133.6
57	7.66	133.6
	7.68	135.1
	7.68	135.8
58	7.70	128.3
59	7.72	132.3
	7.74	125.8
	7.74	128.7

60	7.75	128.7	
	7.80	128.7	
61	7.81	135.7	
62	7.84	133.2	
	7.86	132.8	
	7.86	129.1	
62	7.88	132.3	
63	7.89	127.8	
64	7.92	130.8	
	7.93	129.0	Weak
65	7.95	132.4	
66	7.97	132.8	Weak
67	7.99	131.7	
	7.99	134.1	
	7.99	136.0	
	8.02	123.8	
68	8.03	135.1	
69	8.04	133.2	
	8.04	132.5	
	8.04	133.8	Weak
70	8.09	131.8	
71	8.15	136.1	
	8.16	135.8	
72	8.21	125.6	
	8.22	133.4	
73	8.25	132.9	
	8.26	135.9	
74	8.28	134.6	
	8.30	133.3	
	8.32	132.5	
75	8.37	136.1	
76	8.40	135.0	Weak
77	8.44		
	8.48	133.3	
78	8.57		
	8.83	132.5	
79	9.39		
80	9.46	135.8	
No of resonances		**117**	

Nuclear Overhauser enhancement spectroscopy (NOESY) establishes a through space correlation between neighboring ligands that are within 5-6 Å proximity from one another. In the case of 3-MBA ligand it might also show intra-ligand correlation from H_a to H_{b-d}. Even though the complete ligand structure of Au_{68}(3-MBA) is not known, we can still have some idea which ligands are close to one another.

Some resonances that were clearly visible in the ^1H spectrum (for example 9.39 ppm) did not show cross peaks either in TOCSY or ^{13}C-HSQC spectrum. However, these resonances established strong correlations in the NOESY spectrum suggesting that these resonances could originate either from hydrogen bonded or buried hydroxyl protons.
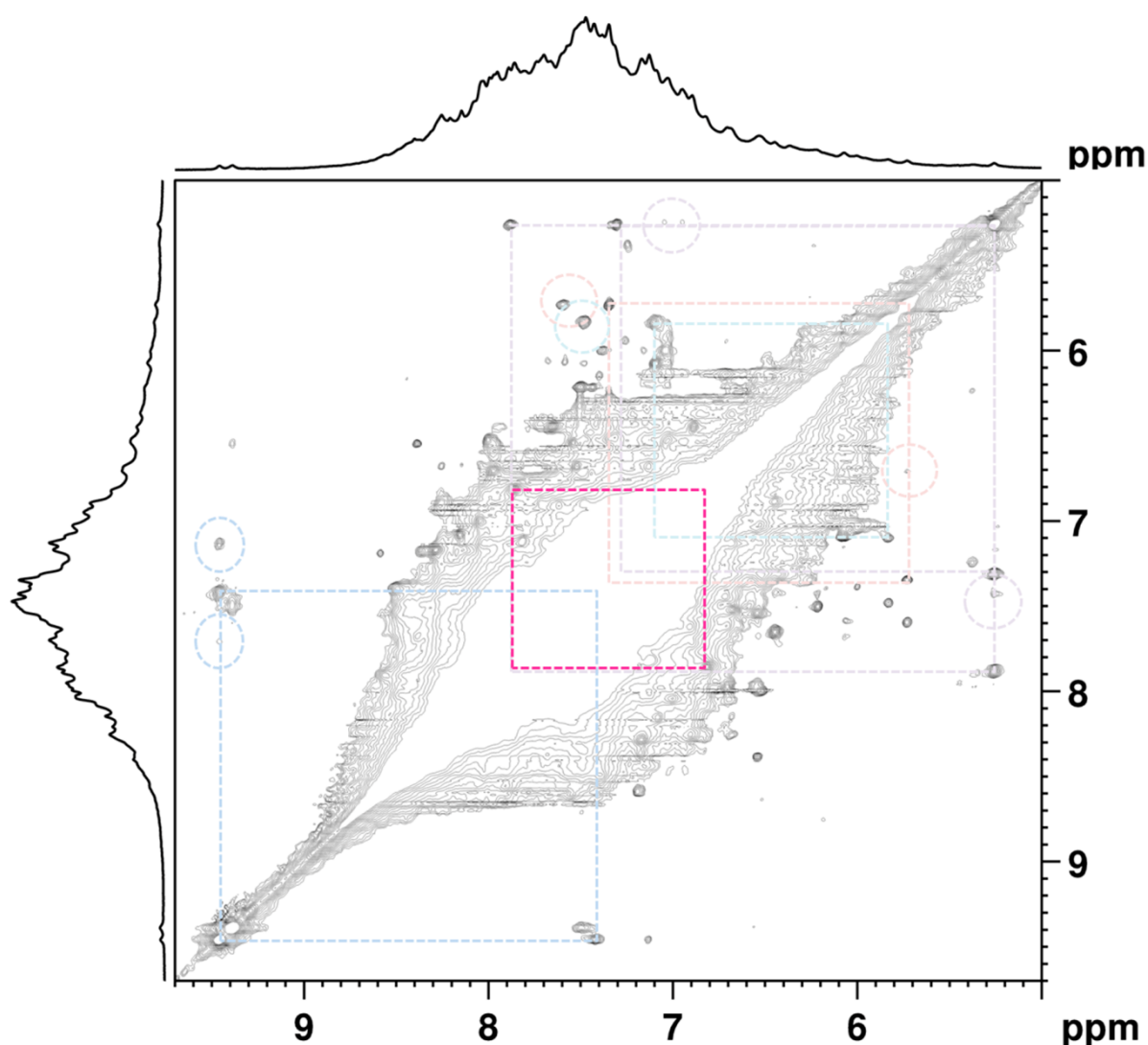

Figure S7. NOESY spectrum of Au_{68}(3-MBA)$_{32}$ in D_2O at 800 MHz. TOCSY correlations of five ligands (ligand no 1, 2, 3, 14 and 23, see Table S4) are highlighted with dashed squares as an example and their spatial correlations are circled.

Table S3. List of resonances from ^{1}H, TOCSY and ^{13}C-HSQC NMR spectra with NOESY correlations. Signals with consecutive numbering were observed in ^{1}H and TOCSY, signals without number were observed from ^{13}C-HSQC and signals written in red were observed from NOESY.

Cross peak no in TOCSY	^{1}H ppm	No of NOESY correlations*	Correlating resonance 1 (ppm)	Correlating resonance 2 (ppm)	Correlating resonance 3 (ppm)	NB
	5.19	0				
1	5.26	3	7.42	6.96	7.04?	
2	5.38	2	6.25	7.25		
	5.60	0				
3	5.73	2	6.71	7.6		
4	5.83	1	7.48			
5	5.90	1	6.29			
6	5.96	1	6.70?			
7	6.01	2	7.04	7.38?		
8	6.08	2	7.58	7.68		
9	6.17	0				
	6.19	1	8.76			Weak
10	6.21	1	7.12			
11	6.25	0				
	6.29	1	5.90			
12	6.33	0				
13	6.37	0				
14	6.42	0				
	6.44	0				
15	6.45	0				
	6.48	0				
	6.52	0				
16	6.54	3	7.99	8.37	7.55	
	6.55	1	7.97			Weak
17	6.63	0				
18	6.67	0				
19	6.68	1	8.15			Weak
	6.68	0				
20	6.70	1	8.25			
21	6.71	1	6.14			Weak
22	6.72	0				
23	6.81	0				
24	6.82	0				
23	6.83	0				
25	6.85	0				
26	6.89	0				
27	6.90	0				
28	6.91	1	8.25			
29	6.93	0				

30	6.96	1	5.25			
	6.97	0				
31	6.99	0				
32	7.02	0				
	7.03	0				
33	7.04	2	6.01	5.26?		
34	7.07	0				
35	7.09	0				
36	7.11	0				
37	7.12	0				
38	7.13	1	9.46			
	7.14	0				
	7.16	1	6.01?		Weak	
39	7.17	0				
40	7.21	1	8.57			
41	7.25	0				
42	7.27	0				
43	7.31	0				
44	7.32	0				
	7.34	0				
45	7.35	0				
	7.36	0				
	7.36	0				
46	7.40	1	8.48		Weak	
	7.42	1	7.86		Weak	
47	7.43	0				
	7.43	0				
48	7.45	1	6.21			
49	7.47	0				
50	7.48	2	5.83	6.08?		
51	7.49	1	9.39			
	7.49	0				
52	7.52	0				
53	7.54	0				
	7.54	0				
	7.54	0				
	7.55	1	6.54			
	7.56	0				
54	7.57	0				
55	7.58	0	6.08			
	7.60	1	5.73			
	7.61	0				
56	7.64	0				
57	7.66	0				
	7.68	0				
	7.68	0				

58	7.70	0				
59	7.72	1	6.42			
	7.74	0				
	7.74	0				
60	7.75	0				
	7.80	0				
61	7.81	0				
62	7.84	0				
	7.86	1	7.42			Weak
	7.86	0				
62	7.88	0				
63	7.89	0				
64	7.92	0				
	7.93	0				
64	7.95	0				
66	7.97	1	6.55			Weak
67	7.99	1	6.54			
	7.99	0				
	7.99	0				
	8.02	1	7.12			
68	8.03	0				
69	8.04	0				
	8.04	0				
	8.04	0				
70	8.09	0				
71	8.15	1	6.68			Weak
	8.16	0				
72	8.21	0				
	8.22	0				
73	8.25	2	6.89	6.68		
	8.26	0				
74	8.28	0				
	8.30	0				
	8.32	0				
75	8.37	0				
76	8.40	0				
77	8.44	1	6.17			Weak
	8.48	0				
78	8.57	1	7.21			
	8.76	1	6.19			Weak
	8.83	0				
79	9.39	2	6.54	7.49		
80	9.46	2	7.13	7.70		

No of resonances   **126**

*in addition to TOCSY correlations which also visible in this measurement

Even though the quality of NMR spectra of Au_{68}(3-MBA)$_{32}$ cluster is very high in comparison to spectra of Au144(3-MBA)$_{40}$ cluster, finding all resonances is very demanding. Since the gold core is asymmetric, most likely there is no symmetry in the ligand layer. The MS results suggested that the cluster has 30-32 ligands meaning 120-128 individual resonances from non-exchangeable protons in ^{1}H NMR. These signals resonate in the aromatic region (5-10 ppm), which is notoriously difficult to assign due to heavily overlapping of ^{1}H chemical shifts. However, asymmetric gold core induces asymmetric ligand layer that is further echoed in surprisingly well-dispersed ^{1}H spectrum.

Indeed, we were able to distinguish 80 resonances (59 of them have TOCSY correlations) from ^{1}H NMR and TOCSY measurement. This number is high enough to confirm the asymmetry of the ligand layer. We obtained 24 different ligands based on their TOCSY correlations (Tables S2 and S4). For nine of these ligands, all H_b, H_c and H_d connectivities were found. H_a does not show cross peaks in the TOCSY spectrum resulting in several resonances exhibiting only autocorrelations. Resonance dispersion in the ^{13}C-HSQC was superior to the TOCSY spectrum partially lifting the ^{1}H resonance degeneracy. Also some signals that did not have correlation in TOCSY correlated to ^{13}C which proved them to be part of the ligand, not just noise. When counting signals from TOCSY and ^{13}C-HSQC the number raised up to 117 signals. This number is already very close to ligand count of 30-32.

The NOESY spectrum showed spatial correlation between some ligands but in addition to that there were correlations between protons that were not distinguished earlier (Table S3, red in color). Interestingly, NOE correlations were seen between protons that did not show correlations in TOCSY or ^{13}C-HSQC spectra but exhibited strong resonance in the ^{1}H spectrum. For example, a strong signal at 9.39 ppm, which does not provide connectivities in the TOCSY or ^{13}C-HSQC, showed spatial correlations to two protons. It is very likely that the resonance at 9.39 ppm belongs to a hydroxyl proton that forms an inter-ligand hydrogen bond and/or is non-accessible to the solvent. In total there are 126 signals that have correlations which means that the number of ligands is in fact 30-32. The number of signals is closer to 128 (32 ligands) than to 120 (30 ligands). Due to the extensive resonance overlap it is very demanding to find all the resonances and to distinguish them from noise. High molecular weight of the system from the NMR studies point of view emphasizes autocorrelation peaks in the TOCSY and NOESY spectra that makes it difficult to find weak cross peaks near the immense diagonal. But since most of the signals have different kinds of correlation, the obtained number can be said to be quite accurate.

Without knowing the ligand structure of the cluster (i.e. crystal structure) it is very difficult if not even impossible to build the absolute structure and specify which signal belongs to which ligand. We were, however, able to connect some of the ligands to their neighboring ligands (Table S4). A schematic presentation shows which ligands are close to one another (Figure S8).

Table S4. Assigned ligands from TOCSY and their NOESY correlations to other ligands. Ligand numbers are only consecutive and they do not refer to any specific ligand.

Ligand no	Proton 1	Proton 2	Proton 3	NB	NOESY correlations to other ligand(s) (ppm)	
1	5.26 (H$_c$)	7.32	7.89		6.96	
2	5.73	6.25	7.35 (H$_c$)		6.71	
3	5.83	7.11			7.48	
4	6.08	7.09			7.58	
5	6.17	7.40				
6	6.21	7.49			7.12	
7	6.37 (H$_c$)	6.67	6.85			
8	6.45 (H$_c$)	6.89	7.66			
9	6.54 (H$_c$)	7.04	7.31	Two signals overlapping?	7.99	8.37
10	6.68 (H$_c$)	7.13	7.52		8.15	9.46
11	6.70	6.93				
12	6.71	7.97				
13	6.72	7.45			6.21	
14	6.81/6.83	7.84/7.88				
15	6.82	6.96			5.26	
16	6.90	7.48			5.83	6.08, weak
17	6.91	7.64				
18	6.99	8.04				
19	7.07	8.15			6.68	
20	7.12 (H$_c$)	7.58	7.81			
21	7.17 (H$_c$)	8.28	8.37			
22	7.25	7.72				
23	7.43	9.46			7.13	
24	7.57 (H$_c$)	7.92	7.99		6.54	
25	?					
26	?					
27	?					
28	?					
29	?					
30	?					
31	?					
32	?					

Figure S8. A schematic visualization of neighboring ligands. Spheres that are overlapping show spatial correlation in NOESY (ligand 4 and 16 have a very weak correlation) and the individual spheres had no correlation to other ligands. The position of spheres in the schematic is not proportional.

Table S5. Full list of ^{1}H NMR signals obtained from different experiments. Each signal has at least one of the correlations measured (TOCSY, HSQC or NOESY, marked as "yes").

^{1}H (ppm)	TOCSY correlation	HSQC correlation	NOESY correlation	^{1}H (ppm)	TOCSY correlation	HSQC correlation	NOESY correlation
5.19		yes		7.43	yes	yes	
5.26	yes	yes	yes	7.43		yes	
5.38			yes	7.45	yes	yes	yes
5.60		yes		7.47		yes	
5.73	yes	yes	yes	7.48	yes	yes	yes
5.83	yes		yes	7.49	yes	yes	yes
5.90		yes	yes	7.49		yes	
5.96		yes		7.52	yes	yes	
6.01		yes	yes	7.54		yes	
6.08	yes	yes	yes	7.54		yes	
6.17	yes			7.54		yes	
6.19			yes	7.55		yes	yes
6.21	yes	yes	yes	7.56		yes	
6.25	yes			7.57	yes	yes	
6.29			yes	7.58	yes	yes	
6.33		yes		7.60		yes	yes
6.37	yes	yes		7.61		yes	
6.42		yes		7.64	yes	yes	
6.44		yes		7.66	yes	yes	
6.45	yes	yes		7.68		yes	
6.48		yes		7.68		yes	
6.52		yes		7.70		yes	
6.54	yes	yes	yes	7.72		yes	yes
6.55			yes	7.74		yes	
6.63		yes		7.74		yes	
6.67	yes	yes		7.75		yes	

Value				Value			
6.68	yes	yes	yes	7.80		yes	
6.68		yes		7.81	yes	yes	
6.70	yes	yes	yes	7.84	yes		
6.71	yes	yes	yes	7.86		yes	yes
6.72	yes			7.86		yes	
6.81	yes	yes		7.88	yes	yes	
6.82	yes	yes		7.89	yes	yes	
6.83				7.92	yes	yes	
6.85	yes			7.93		yes	
6.89	yes	yes		7.95		yes	
6.90	yes	yes		7.97	yes	yes	
6.91	yes		yes	7.99	yes	yes	yes
6.93	yes	yes		7.99		yes	
6.96	yes	yes	yes	7.99		yes	
6.97		yes		8.02		yes	yes
6.99	yes			8.03		yes	
7.02	yes	yes		8.04	yes	yes	
7.03		yes		8.04		yes	
7.04	yes	yes	yes	8.04		yes	
7.07	yes	yes		8.09		yes	
7.09	yes	yes		8.15	yes	yes	yes
7.11	yes	yes		8.16		yes	
7.12	yes	yes		8.21		yes	
7.13	yes	yes	yes	8.22		yes	
7.14		yes		8.25		yes	yes
7.16		yes	yes	8.26		yes	
7.17	yes	yes		8.28	yes	yes	
7.21			yes	8.30		yes	
7.25	yes	yes		8.32		yes	
7.27		yes	yes	8.37	yes	yes	
7.31	yes	yes		8.40	yes	yes	
7.32	yes	yes		8.44			yes
7.34		yes		8.48		yes	
7.35	yes	yes		8.57			yes
7.36		yes		8.76			yes
7.36		yes		8.83		yes	
7.40	yes	yes	yes	9.39			yes
7.42		yes	yes	9.46	yes	yes	yes

B. MODELING STRATEGIES AND STATISTICS OF MD DATA

Building the initial structures for MD simulations: The initial structures of the ligand layer were created by an in-house algorithm that uses the knowledge of Au-S-interface from the known protected Au-nanoparticles. A set of reference structures can include known experimental structures, well established computational model structures or any structure that is expected to describe Au-S-interface of the unknown structure. After the Au-atom coordinates of the unkown structure have been read, the algorithm found the allowed positions for S-atoms close to the Au-atoms. Criteria to select an allowed S-atom position is based on the nearest neighbor Au-S-distances, Au-S coordination and Au-S bond angles.

After determining a set of allowed S-atom positions, the process continued by a random selection of the allowed S-atom positions one-by-one. After selecting one S-atom position the set of allowed positions is reprocessed to neglect all the S-atom positions that are for example too close to the already selected S-atoms. The allowed positions were also reprocessed to ensure that no Au-atom binds more than two S-atoms with a given distance range. Random selection of the S-atom positions continued until no allowed points are left that would obey the given criteria. Random selection of S-atom positions can be also tuned to favor formation of SR-Au-SR units on the surface.

After generating one model with Au- and S-atom positions, the PhCOOH moieties were added. If the natural Au-S-C angle could not be accommodated (leading to steric overlap in the ligand layer), the initial orientation of the organic group pointed radially out from the center of mass of the gold core. This process could lead to a small number of overlapping ligands, in which case the MD simulations were started by gradually switching on the ligand-ligand force field. Several model clusters were created from the allowed S-atom positions using the same procedure, from which representative model structures were selected for MD-simulations and final phase of modeling.

Details of the MD simulations. We performed molecular dynamics simulations with Gromacs 5.0.4 (ref. 1) for 3 model structures of $Au_{68}(3\text{-MBA})_{32}$ nanocluster with different ligand positions, and 7 model structures of $Au_{144}(3\text{-MBA})_x$ with varying number of ligands (x=40-53). AMBER force field parameters for 3-MBA and gold were obtained as described in ref. 2. Due to the lack of information on the structural motifs of the ligand shell, only bonded and no angle parameters were used to describe the Au-S interface in this work. In constructing the bonds, each sulfur was connected to two closest gold atoms within a certain cut-off distance and requiring each gold atom connects to maximum of 2 sulfur atoms. Also 'open units' (i.e. sulfur connects to only one Au atom) were allowed in cases where there was only one close gold atom. The simulations were performed in 3 different protonation states of the ligand shell for each structure, with 0 %, 20-25 % and 40-50 % of the 3-MBA ligands randomly deprotonated. Simulations were performed in TIP3P water with neutralizing counter ions (Na). For $Au_{144}(3\text{-MBA})_{53}$ model, also 75 % and 100 % deprotonation states were simulated. To investigate the effect of the protonation pattern, two simulations with different random deprotonation patterns of deprotonated states 25-75 % were performed for $Au_{144}(3\text{-MBA})_{53}$ and $Au_{144}(3\text{-MBA})_{49}$ models. In addition, $Au_{144}(3\text{-MBA})_x$ models were simulated in methanol in fully protonated form. Methanol (GAFF) parameters and structure were obtained from Virtualchemistry website (refs. 3,4).

The positions of the gold atoms were fixed in all simulations to the TEM structure. To remove ligand overlaps of the initial structures, 20 ps simulations where interactions were gradually turned on were performed (separately) 5 times for each $Au_{68}(3\text{-}MBA)_{32}$ model and 10 times for each $Au_{144}(3\text{-}MBA)_x$ model. In the switching simulations, a stochastic integrator was used with time step of 1 fs, periodic boundary conditions, a 1.0 nm Lennard-Jones cut-off with dispersion correction for energy and pressure, PME electrostatics with a 1.0 nm cut-off and 0.12 nm grid spacing, the velocity-rescale thermostat with a reference temperature of 300 K and coupling time constant of 0.1 ps. All bond lengths were constrained with the LINCS algorithm. Random velocities were generated at the start of each switching, where GROMACS lambda-integration was utilized to gradually turn on non-bonded interactions using soft-core alpha, sigma and power parameters 0.5, 0.3 and 1, respectively. 50 ns production NPT simulations were then initiated from each of the switched structures with similar simulation setup, but now using leap-frog integrator with 2 fs timestep and in addition Berendsen barostat with a reference pressure of 1 bar and coupling time constant of 1 ps with all interactions on.

Taking into account all variations in the ligand count, initial configurations of the ligand layer, and the few different protonation states for a given composition, and two solvents (water and methanol), the total number of simulated models is of the order of 300.

system	# deprot. ligands	hb ligand-ligand (total)	aromatic contacts (/ligand)	Au-lig contacts (total)	syn/ syn-close/ anti/ anti-close (%)	flat lying ligands
$Au_{68}3MBA_{32}1$	0	0.06	1.45	3.93	87/ 9/ 3/ 1	1.78
$Au_{68}3MBA_{32}1$	6	1.82	1.44	2.93	89/ 7/ 3/ 1	1.51
$Au_{68}3MBA_{32}1$	13	1.54	1.45	3.48	84/ 11/ 3/ 2	1.71
$Au_{68}3MBA_{32}3$	0	0.19	1.38	3.20	87/ 7/ 3/ 3	2.35
$Au_{68}3MBA_{32}3$	6	0.29	1.41	3.45	87/ 7/ 4/ 2	2.62
$Au_{68}3MBA_{32}3$	13	1.85	1.38	2.88	86/ 10/ 3/ 1	2.11
$Au_{68}3MBA_{32}6$	0	0.08	1.48	4.07	90/ 6/ 2/ 2	3.46
$Au_{68}3MBA_{32}6$	6	1.66	1.52	3.22	90/ 6/ 2/ 2	2.65
$Au_{68}3MBA_{32}6$	13	1.59	1.47	3.54	94/ 3/ 2/ 1	2.58
$Au_{144}3MBA_{40}$	0	0.55 [1.19]	1.35 [1.38]	4.35 [3.24]	91/ 6/ 1/ 2 [85/ 7/ 3/ 5]	3.40 [2.34]
$Au_{144}3MBA_{40}$	10	2.27	1.38	3.92	93/ 2/ 3/ 2	3.16
$Au_{144}3MBA_{40}$	20	2.58	1.30	4.15	92/ 5/ 2/ 1	3.43
$Au_{144}3MBA_{42}$	0	0.67 [0.97]	1.32 [1.31]	4.15 [3.88]	90/ 7/ 2/ 1 [82/ 8/ 5/ 5]	3.19 [2.99]
$Au_{144}3MBA_{42}$	10	2.46	1.34	3.85	85/ 10/ 3/ 2	3.08
$Au_{144}3MBA_{42}$	21	3.66	1.38	4.32	87/ 8/ 4/ 1	3.30
$Au_{144}3MBA_{44}$	0	0.28 [0.35]	1.43 [1.47]	2.16 [1.88]	91/ 4/ 3/ 2 [78/ 6/ 9/ 7]	1.77 [1.50]
$Au_{144}3MBA_{44}$	11	2.13	1.46	3.58	90/ 4/ 5/ 1	2.82
$Au_{144}3MBA_{44}$	22	5.42	1.40	1.87	86/ 4/ 8/ 2	1.48
$Au_{144}3MBA_{47}$	0	0.36 [0.88]	1.47 [1.56]	3.04 [3.01]	89/ 7/ 2/ 2 [78/ 10/ 7/ 5]	1.77 [1.37]
$Au_{144}3MBA_{47}$	11	3.72	1.50	2.93	90/ 6/ 2/ 2	1.91
$Au_{144}3MBA_{47}$	23	2.66	1.46	2.15	89/ 6/4/ 1	1.00
$Au_{144}3MBA_{49}$	0	0.55 [0.90]	1.54 [1.67]	2.69 [2.68]	89/ 3/ 4/ 4 [74/ 6/ 9/ 11]	1.19 [1.33]
$Au_{144}3MBA_{49}$	12	1.90 (2.97)	1.55 (1.57)	3.74 (2.06)	88/ 3/ 6/ 3 [86/ 4/ 6/ 4]	1.67 (0.75)
$Au_{144}3MBA_{49}$	24	5.00 (3.46)	1.57 (1.55)	2.80 (2.00)	91/ 2/ 5/ 2 (92/ 5/ 2/ 1)	1.19 (0.89)
$Au_{144}3MBA_{51}$	0	0.32 [1.04]	1.63 [1.71]	3.30 [3.06]	85/ 7/ 5/ 3 [74/ 11/ 10/ 5]	1.42 [1.37]
$Au_{144}3MBA_{51}$	12	2.91	1.61	2.06	83/ 6/ 8/ 3	1.08
$Au_{144}3MBA_{51}$	25	2.53	1.63	2.55	82/ 9/ 7/ 2	1.20
$Au_{144}3MBA_{53}$	0	0.32 [0.55]	1.67 [1.79]	2.93 [3.65]	82/ 7/ 6/ 5 [69/ 8/ 13/ 10]	1.60 [2.06]
$Au_{144}3MBA_{53}$	13	2.34 (2.50)	1.67 (1.68)	2.35 (3.11)	87/ 5/ 5/ 3 (84/ 5/ 7/ 4)	1.40 (1.79)
$Au_{144}3MBA_{53}$	26	3.66 (2.88)	1.70 (1.63)	2.52 (2.23)	84/ 9/ 6/ 1 (83/ 7/ 5/ 5)	1.54 (0.94)
$Au_{144}3MBA_{53}$	39	2.28 (2.42)	1.63 (1.62)	1.72 (1.61)	82/ 9/ 7/ 2 (81/ 11/ 6/ 2)	0.60 (1.0)
$Au_{144}3MBA_{53}$	53	–	1.60	1.36	–	0.52

$Au_{144}pMBA_{41}$	0	0.14	1.41	1.23	92/0/8/0	0.51
$Au_{144}pMBA_{41}$	20	1.01	1.36	1.70	78/0/20/2	0.74
$Au_{144}pMBA_{41}$	41	–	1.25	1.32	–	0.43
$Au_{144}pMBA_{60}$	0	0.02	1.93	2.8	92/0/8/0	0.99
$Au_{144}pMBA_{60}$	15	0.11	2.01	1.47	82/0/18/0	0.46
$Au_{144}pMBA_{60}$	30	0.16	1.95	0.45	73/0/1/26	0.07
$Au_{102}pMBA_{32}$	0	0.18	1.38	2.45	92/0/8/0	1.18
$Au_{102}pMBA_{32}$	16	1.43	1.35	3.86	74/0/25/1	1.53
$Au_{102}pMBA_{32}$	32	–	1.23	2.95	–	0.93
$Au_{102}pMBA_{44}$	11	0.51	1.92	5.64	91/0/9/0	1.94
$Au_{102}pMBA_{44}$	22	0.52	1.77	2.51	78/0/22/0	1.14
$Au_{102}pMBA_{44}$	33	0.21	1.75	2.11	67/0/33/0	0.94
$Au_{102}pMBA_{44}$	44	–	1.64	0.57	–	0.08

Table S6. Averages from 1-10 simulations of 50 ns. Results in methanol are presented in square brackets [] and the results for an alternative deprotonation pattern in (). The number after $Au_{68}(3\text{-}MBA)_{32}$ systems denotes the model structure number (i.e., different ligand positions). Hydrogen bonds between ligands were analyzed using GROMACS gmx hbond tool with default settings of cutoff angle of 30 degrees and cutoff distance 0.35 nm. Aromatic contacts were estimated by requiring centers of mass of ligands being closer than 0.7 nm of each other for a contact to form. Au-lig contacts show number of contacts within 0.2 nm between any ligand atom and a gold atom (contains some of the close-syn/anti contacts and flat lying ligands). Syn/ syn-close/ anti/ anti-close show percentages of each of these forms of the COOH-group containing ligands during the 50 ns simulation. Syn-close and anti-close forms occur when the HO hydrogen lies closer than 0.28 nm of a gold atom. Flat lying ligands show number of ligands whose ring center of mass lies closer than 0.28 nm of a gold atom.

C. IR-SPECTROSCOPY OF 3-MBA

C1. SAMPLE PREPARATION
The 3-MBA was weighed with the precision of ± 0.001 g and then directly dissolved in deuterated-methanol or CCl_4. The methanol samples were shaken in Eppendorf tubes for 2 minutes at 2500 rpm. The halogen containing solvent samples were only exposed to glassware, in which they had been stirred with magnetic stirrer for two hours due to limited solubility. The water-soluble partially-deprotonated gold clusters were first dissolved in D_2O for NMR and UV/vis measurements. For the IR measurements the sample was diluted, and approximately 20 v/v% concentrated HCl excess acid was added to fully protonate the clusters. Protonation results in phase separation, and a black precipitate formed. It was transferred to a 5 ml Erlenmeyer, from which the water was evaporated applying moderate vacuum. The dry precipitate was dissolved in a 1% DCl-D_2O / MeOD mixture and IR measurements were instantly performed.

C2. 3-MBA IN CCL$_4$
Determination of the ligand states in clusters requires accurate knowledge on the effects of hydrogen bonding and various conformations on their spectroscopic properties. Therefore, in the first place, the dimerization of the pure ligand was studied, in both aprotic and protic solvents.

The two, distinct characteristic IR absorption bands of carboxylic acids, O−H stretching and C=O stretching band, are both very sensitive to hydrogen bonding. Thus, dimer formation gives rise to new absorption bands at different positions in the spectrum, as new bonding environment is formed. The O−H stretching and the antisymmetric C=O stretching of the dimer are IR active, which makes them good candidates for following the dimerization process. We first dissolved 3-MBA in CCl_4. In the IR spectrum two pairs of absorption bands in the regions $3600 - 2500$ cm^{-1} and $1750 - 1650$ cm^{-1} can be identified, as can be seen in Supplementary Figure 9a. The intensity ratio of the bands is concentration dependent. In the region of the C=O stretching vibration modes two high intensity peaks at 1744 cm^{-1} and 1699 cm^{-1} are present. The relative intensity of the latter peak increases upon increasing concentration of 3-MBA. Therefore, these absorption bands can be assigned to the stretching vibration of C=O double bond of the monomer and dimer, respectively. A similar tendency can be found between two spectral features at higher wavenumbers. A narrow small intensity peak at 3537 cm^{-1} (see Inset of Supplementary Figure 9a) loses intensity relative to the broad absorption between 3300-2400 cm^{-1} as concentration grows. The very characteristic absorption at 3537 cm^{-1} belongs to the O−H stretching mode of the free 3-MBA monomers, while the equivalent vibration mode of the dimer is redshifted and broadened due to hydrogen bonding. The assignment is in good accordance with the conclusions of previous studies [3-4], which also suggests approximately 40-50 cm^{-1} difference between the C=O stretching modes of monomers and dimers of benzoic-acid derivatives, with dimers having lower frequency.

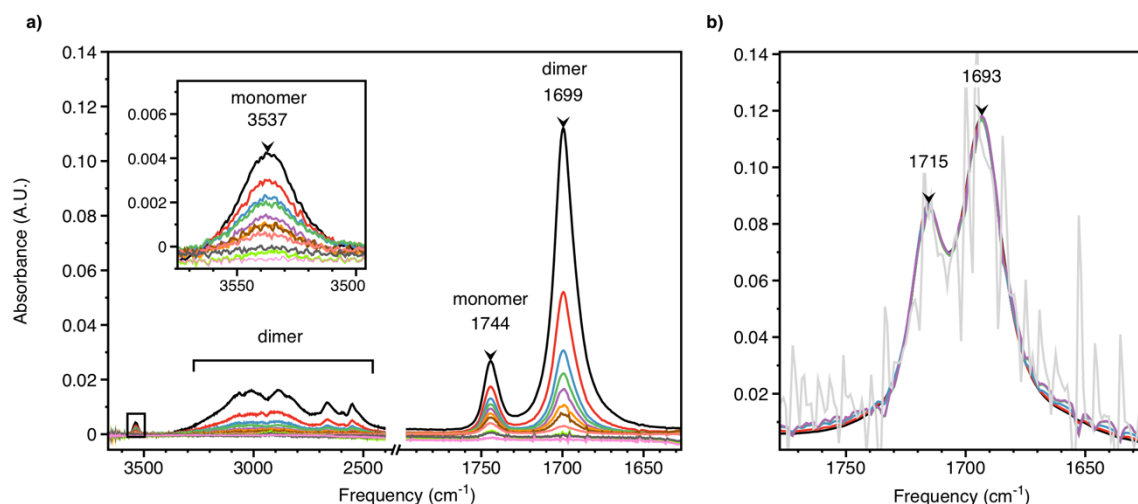**Figure S9. a)** IR spectra of dilution series of 3-MBA dissolved in CCl$_4$. Concentrations are *(● black)* 2.6461 mM, *(● red)* 1.3230 mM, *(● blue)* 0.8820 mM, *(● green)* 0.6615 mM, *(● purple)* 0.5292 mM, *(● orange)* 0.3528 mM, *(● brown)* 0.2646mM, *(● salmon)* 0.1323 mM, *(● neongreen)* 0.08820 mM, *(● grey),* 0.05292 mM, *(● pink)* 0.02646 mM **b)** IR spectra from a dilution series of 3-MBA dissolved in MeOD scaled to the highest concentration. Original concentrations are: *(● black)* 0.130 M, *(● red)* 0.065 M, *(● blue)* 0.032 M, *(● green)* 0.019 M, *(● purple)* 0.006 M, *(● grey),* 0.002 M.

From this data the equilibrium constant (K = 1.51 X 10^4 l/mol) and the standard Gibbs-free energy ($\Delta_r G° = $ -23.8 kJ/mol) of the reaction (dimerization) were determined.

C3. 3-MBA IN METHANOL

It is expected that when 3-MBA is dissolved in protic solvents, hydrogen bonding with solvent molecules will also occur, and this will compete with the solute-solute hydrogen bonding, a.k.a. dimerization. Indeed, the observations indicate remarkably different behaviour from CCl$_4$. As shown in Figure S9b, the IR spectrum of 3-MBA dissolved in deuterated methanol features a doublet peak in the carbonyl stretch region with peak positions of 1715 cm^{-1} and 1694 cm^{-1}. This is very similar to what has been observed previously for *p*-MBA ligand [5]. In order to resolve the origin of the doublet, we studied the concentration dependence of the peak intensities. As seen in Figure S9b, the results show no concentration dependence for the relative intensities, contrary to what is found in CCl$_4$. The normalised spectra completely overlap for concentration range from 0.130 mol dm^{-3} to 0.002 mol dm^{-3}. Thus, we conclude that the doublet belongs solely to the monomer providing a sound basis to rule out the dimer formation in protic solvents.

In order to explain the origin of the doublet peak, we consider conformational isomerism in carboxylic acids. It is well known that carboxylic-acids can adopt two spatial arrangements in the preferable planar geometry, through the intramolecular rotation of the C-O bond [8-11]. In these conformations the R$_1$-C-O-H torsion angle is either 0 or 180 degrees. In references 8 – 11, *cis* and *trans* terms were used for these conformers corresponding to 0 and 180 degrees dihedral angles, respectively. Since in literature also opposite convention is sometimes used, we use here *syn* and *anti* nomenclature, corresponding to 180 and 0 degrees R$_1$-C-O-H angles (or 0 and 180 ° O=C-O-H angles), respectively. In the absence of any strong interaction involving one or both R groups, the *syn* conformer has the lower energy. The energy difference is so large that usually it will be the

solely dominating species at room temperature in the gas phase [8-11]. On the other hand, it is known that strong intramolecular hydrogen bonding can make the *syn* form the conformational ground state[10-13]. This leads to the idea that intermolecular (solute-solvent) hydrogen bonding can change significantly the energetics. Thus, we suggest that the peaks observed in MeOD at 1715 cm^{-1} and 1694 cm^{-1} correspond to C=O stretching mode of monomeric 3-MBAs, but to the *anti* and *syn* conformers respectively. This assignment is both supported by the fact, that the frequency difference of 21 cm^{-1} of carbonyl group stretching frequency is close to the difference found in matrix-isolation studies of small carboxylic acids (25-30 cm^{-1}) [15], and to the 22 cm^{-1} observed for benzoic acid in argon matrices [5].

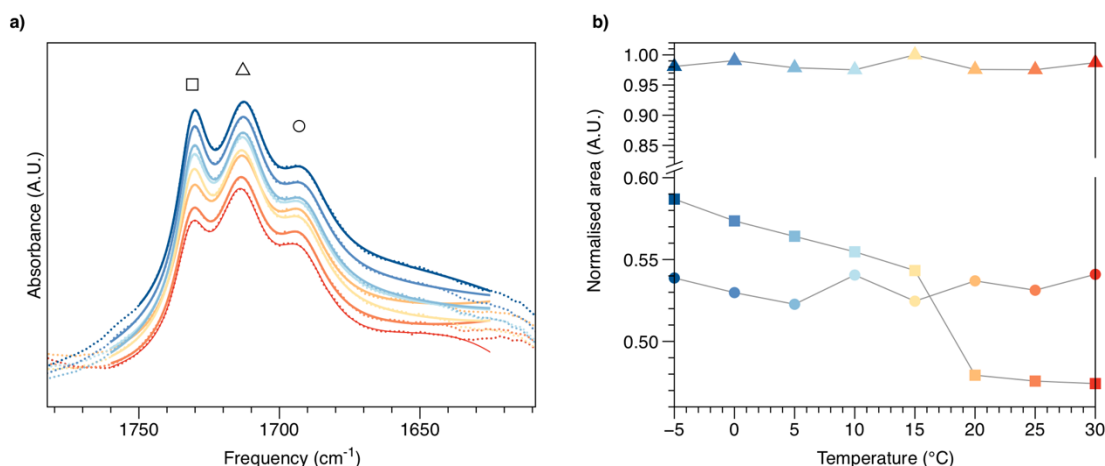## D. TEMPERATURE-DEPENDENT IR SPECTRA OF Au_{68} AND Au_{144}
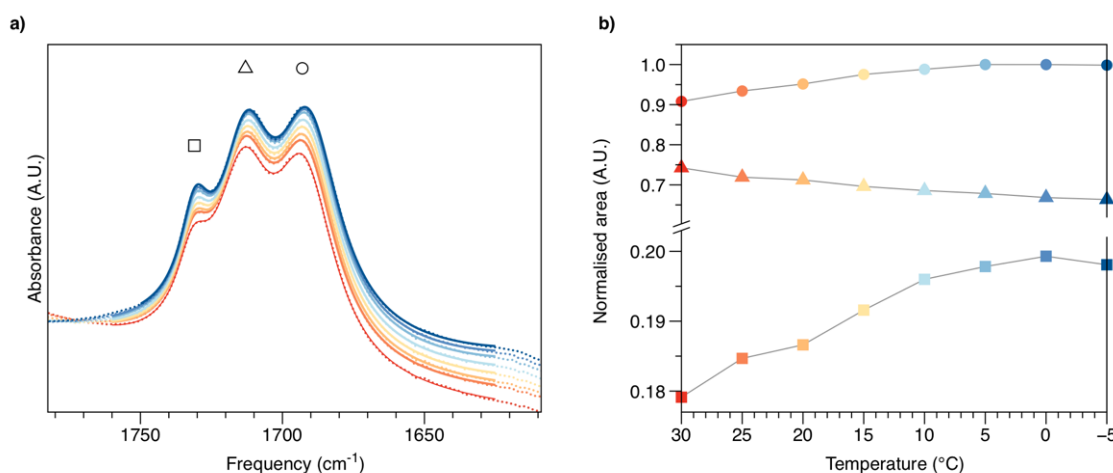
Figure S10: IR-spectrum in the carbonyl stretch region of Au_{68}(3-MBA)$_{32}$ cluster measured at different temperatures. Temperature coloring: (●) 30 °C, (●) 25 °C, (●) 20 °C, (●) 15 °C, (●) 10 °C, (●) 5 °C, (●) 0 °C, (●) -5 °C. The dotted lines represent the experimental data, and the solid lines are the fitted sum of three Lorentzians and a 5th order polynomial. **b)** The normalised peak areas of the peaks at 1731 cm^{-1} (squares), 1714 cm^{-1} (triangles) and 1695 cm^{-1} (circles) of the Au_{68}(3-MBA)$_{32}$ cluster at different temperatures, as obtained from fitting.

Figure S11 a) IR-spectrum in the carbonyl stretch region of $Au_{144}(3\text{-MBA})_{\sim 40}$ cluster measured at different temperatures. Temperature coloring: (•) 30 °C, (•) 25 °C, (•) 20 °C, (•) 15 °C, (•) 10 °C, (•) 5 °C, (•) 0 °C, (•) -5 °C. The dotted lines represent the experimental data, and the solid lines are the fitted sum of three Lorentzians and a 5th order polynomial. **b)** The normalised peak areas of the peaks at 1731 cm^{-1} (squares), 1714 cm^{-1} (triangles) and 1695 cm^{-1} (circles) of the $Au_{144}(3\text{-MBA})_{\sim 40}$ cluster at different temperatures, as obtained from fitting.

E. IR SPECTRUM OF $Au_{68}(3\text{-MBA})_{32}$ IN WATER UNDER VARIOUS pH CONDITIONS

The FTIR spectrum of the $Au_{68}(3\text{-MBA})_{32}$ cluster was measured in D_2O with 80 μm optical path length. The pH of the solution was tuned with DCl and NaOD solutions to determine the pH dependence of the spectrum. All spectra were corrected for residue H_2O by subtracting the spectrum of H_2O measured in D_2O. The protonated cluster is insoluble in water and at pH 5.3 some of the cluster sample was visibly precipitated.

At high pH the cluster is fully deprotonated (similarly to the previously studied $Au_{102}(p\text{-MBA})_{44}$, see ref. 7), which is clearly indicated by the lack of carbonyl group stretching vibration peak at ~1685 cm^{-1}. As the pH decreases, this peak becomes more pronounced indicating an increasing degree of protonation of the clusters 3-MBA ligands. Unlike in methanol, no distinct peaks can be found within this band, due to band broadening in D_2O when compared to MeOD, similarly to earlier studies with p-MBA (ref. 7).
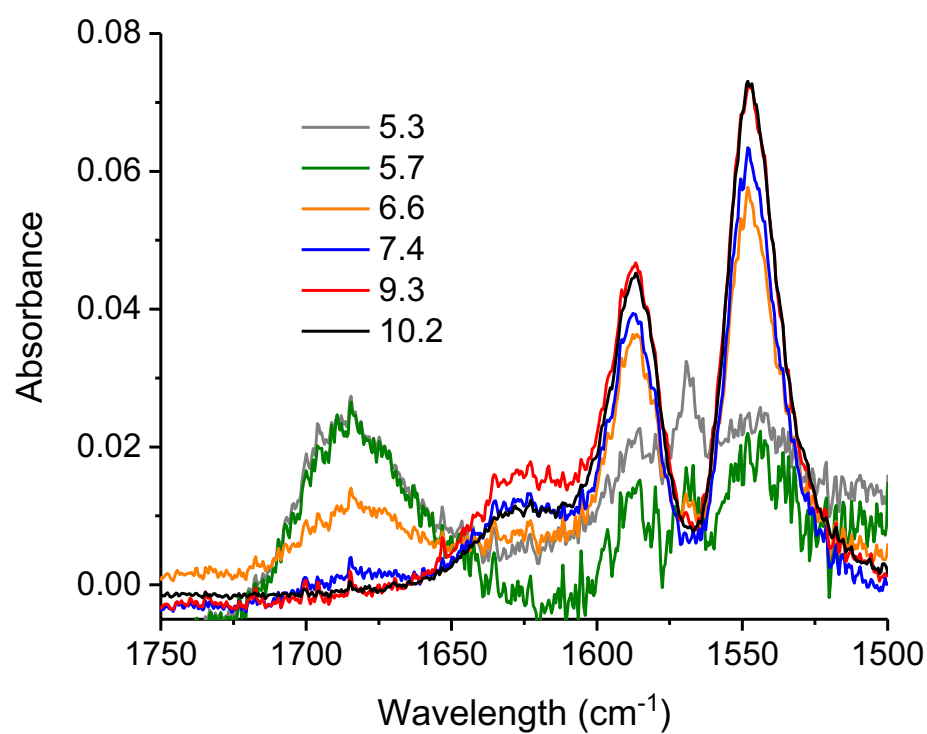
Figure S12. IR-spectrum of $Au_{68}(3\text{-MBA})_{32}$ in D_2O in the range of pH values from 5.3 to 10.2.

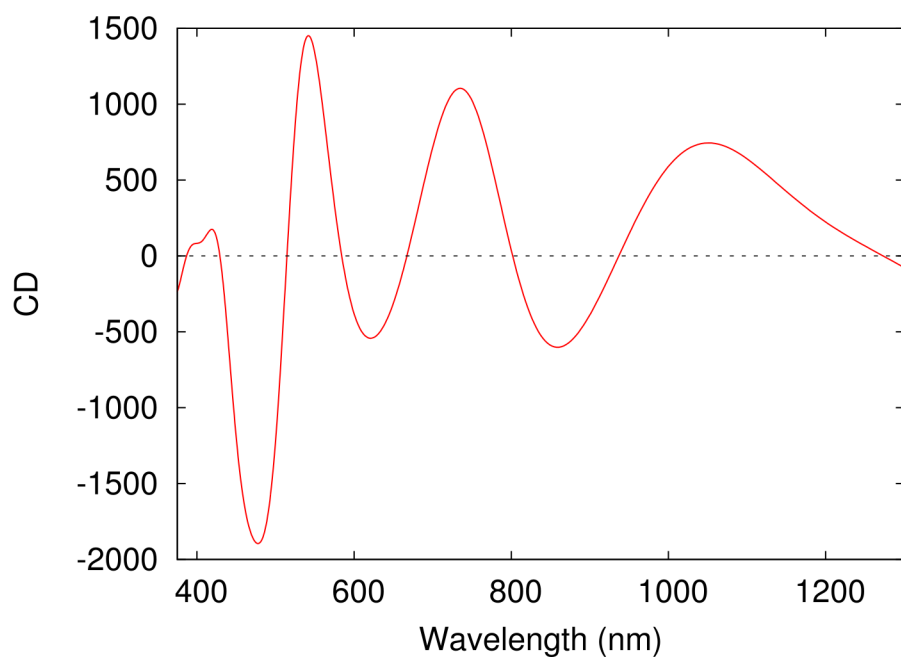# F. OPTICAL ACTIVITY OF $Au_{144}(3\text{-MBA})_{40}$

Figure S13. The computed CD spectrum of the $Au_{144}(3\text{-MBA})_{40}$ model cluster.

G. REACTIONS BETWEEN 3-MBA-STABILIZED GOLD NANOCLUSTERS AND THIOL-MODIFIED DNA
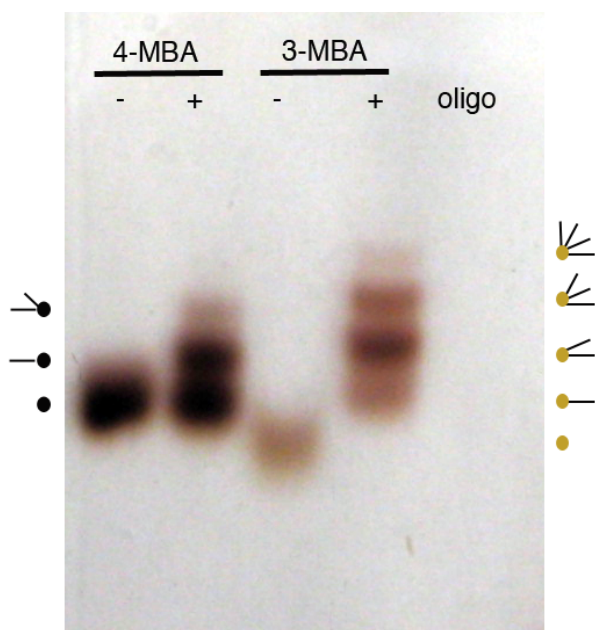

Figure S14. Reactivity of 4-MBA protected (left) and 3-MBA protected (right) gold nanoclusters towards thiol-modified oligodeoxynucleotides. After the conjugation reaction, 4-MBA protected clusters exhibit PAGE bands both for the original unreacted cluster and the reacted cluster with one or two oligonucleotides, while for 3-MBA protected clusters, the original unreacted cluster band disappears and the system displays up to four distinct new bands, reflecting successful conjugation reactions up to four oligonucleotides. This indicates profoundly different reaction mechanisms in the 4-MBA and 3-MBA protected clusters. For more details see ref. 5 and our discussion in the main text. Reproduced with permission from ref. 5 in the main text. Copyright 2016 American Chemical Society.

H. LIST OF Au COORDINATES OF Au$_{144}$(3-MBA)$_{\sim40}$ FROM ELECTRON MICROSCOPY (M. Azubel and R.D. Kornberg, private communication)

Au	-0.103000	2.334000	4.919000
Au	5.395000	3.012000	3.822000
Au	1.668000	-2.014000	2.695000
Au	1.448000	1.271000	6.844000
Au	0.677000	0.368000	9.783000
Au	2.808000	-0.172000	4.323000
Au	3.277000	-0.376000	9.875000
Au	2.671000	2.594000	4.121000
Au	1.399000	-1.773000	8.013000
Au	2.558000	-2.527000	5.652000
Au	4.310000	-2.823000	2.780000
Au	1.300000	0.876000	2.250000
Au	3.563000	-0.407000	7.115000
Au	4.954000	0.656000	11.788000
Au	5.330000	1.199000	8.931000
Au	-1.096000	0.311000	7.319000
Au	-4.082000	-0.767000	7.898000
Au	5.876000	-1.325000	10.194000
Au	-0.089000	0.249000	12.410000
Au	2.355000	1.784000	11.615000
Au	0.098000	-3.576000	6.259000
Au	3.991000	2.231000	6.483000
Au	-2.468000	-1.345000	5.421000
Au	6.806000	5.077000	5.776000
Au	6.301000	-0.300000	6.860000
Au	0.788000	1.462000	-0.528000
Au	-1.322000	5.271000	6.123000
Au	5.214000	3.311000	1.176000
Au	5.258000	-2.292000	5.269000
Au	4.047000	-2.810000	8.311000
Au	0.131000	-0.636000	5.018000
Au	4.001000	0.896000	1.981000
Au	3.531000	1.426000	-0.752000
Au	5.501000	0.310000	4.269000
Au	1.415000	4.167000	6.328000
Au	0.741000	-3.798000	0.891000
Au	7.655000	1.547000	11.160000
Au	7.013000	-2.460000	2.484000
Au	2.772000	5.903000	7.926000
Au	-1.817000	-4.722000	1.244000
Au	3.285000	-4.707000	0.952000
Au	2.290000	-4.463000	3.755000
Au	-3.474000	-3.122000	3.591000
Au	-1.861000	1.422000	9.661000
Au	-0.546000	-3.689000	3.632000
Au	5.926000	-4.145000	0.653000

Au	-1.256000	-2.298000	8.276000
Au	9.019000	-0.831000	7.006000
Au	8.576000	-0.825000	9.683000
Au	-1.916000	-1.158000	10.642000
Au	6.670000	2.384000	6.128000
Au	6.642000	2.155000	13.671000
Au	9.830000	-2.114000	2.321000
Au	0.470000	4.048000	2.866000
Au	0.179000	6.800000	8.011000
Au	8.090000	1.560000	8.495000
Au	7.939000	-2.710000	5.355000
Au	1.386000	6.742000	5.464000
Au	-0.490000	5.409000	0.695000
Au	1.433000	7.534000	2.867000
Au	8.169000	0.755000	3.972000
Au	-2.576000	-3.954000	6.353000
Au	-0.694000	3.000000	7.561000
Au	1.583000	1.862000	14.293000
Au	10.279000	0.948000	11.590000
Au	-1.671000	1.490000	2.764000
Au	11.152000	-0.083000	4.053000
Au	3.155000	3.115000	8.892000
Au	3.380000	-1.922000	-0.073000
Au	2.555000	-4.822000	7.140000
Au	8.214000	3.808000	3.416000
Au	4.070000	5.168000	5.631000
Au	6.639000	3.978000	8.533000
Au	-0.929000	-1.221000	2.492000
Au	10.656000	-2.647000	5.013000
Au	-0.182000	2.867000	11.282000
Au	1.198000	-2.971000	10.696000
Au	0.738000	-6.189000	2.267000
Au	-1.820000	0.760000	0.122000
Au	2.459000	6.132000	10.859000
Au	0.812000	4.485000	9.361000
Au	-4.966000	-0.237000	5.367000
Au	9.549000	2.026000	5.961000
Au	5.408000	-4.565000	6.753000
Au	-4.678000	1.888000	3.295000
Au	2.685000	-0.818000	12.498000
Au	9.581000	4.776000	5.539000
Au	5.468000	3.150000	10.849000
Au	2.390000	-0.991000	-2.472000
Au	-2.039000	5.404000	8.890000
Au	3.729000	5.921000	2.516000
Au	7.839000	2.637000	1.001000
Au	-5.348000	-2.958000	6.091000
Au	5.655000	7.006000	7.437000
Au	-0.131000	6.949000	10.903000
Au	6.357000	1.088000	-0.828000

Au	8.547000	-3.458000	0.295000
Au	-3.602000	-3.551000	8.826000
Au	6.887000	-2.812000	8.176000
Au	11.734000	-0.861000	6.776000
Au	-0.255000	-0.446000	-2.292000
Au	8.149000	-4.999000	6.828000
Au	1.432000	4.434000	12.859000
Au	9.199000	3.109000	13.129000
Au	6.289000	3.776000	-1.322000
Au	4.106000	2.056000	14.040000
Au	3.507000	-6.878000	2.542000
Au	-4.626000	-2.164000	10.949000
Au	3.915000	-6.178000	5.154000
Au	5.486000	7.167000	4.387000
Au	-2.833000	3.424000	4.770000
Au	8.998000	-4.503000	3.619000
Au	9.150000	-3.969000	9.172000
Au	5.241000	6.763000	10.244000
Au	5.420000	-2.216000	12.726000
Au	2.723000	7.836000	0.508000
Au	4.102000	5.338000	-0.865000
Au	10.791000	2.534000	3.446000
Au	5.118000	-0.202000	-2.939000
Au	2.488000	3.897000	1.077000
Au	-4.319000	0.452000	10.314000
Au	6.912000	-6.577000	4.998000
Au	2.518000	-3.656000	-2.015000
Au	8.404000	6.785000	7.435000
Au	5.309000	-2.914000	-2.421000
Au	6.353000	-1.578000	-0.271000
Au	9.490000	0.568000	1.590000
Au	3.870000	-4.819000	10.172000
Au	-3.077000	-0.984000	13.085000
Au	2.138000	1.687000	-3.174000
Au	7.369000	-5.775000	-1.295000
Au	-0.351000	-4.821000	8.784000
Au	0.618000	-1.173000	0.177000
Au	5.858000	-8.155000	3.052000
Au	-3.592000	-0.578000	2.663000
Au	-2.787000	1.740000	12.303000
Au	-6.189000	-1.972000	3.548000
Au	5.286000	7.095000	0.816000
Au	9.708000	3.433000	10.394000
Au	-0.139000	-4.060000	-1.668000
Au	-2.982000	-0.400000	-2.138000
Au	-3.818000	-2.889000	0.913000
Au	10.718000	0.834000	8.718000
Au	4.700000	-5.363000	-1.457000

I. REFERENCES

[1] Abraham, M.J.; Murtola, T.; Schulz, R.; Páll, S.; Smith, J.C.; Hess, B.; Lindahl, E. Gromacs: High Performance Molecular Simulations Through Multi-Level Parallelism from Laptops to Supercomputers. *SoftwareX* **2015**, *1–2*, 19 – 25.

[2] Pohjolainen, E.; Chen, X.; Malola, S.; Groenhof, G.; Häkkinen, H. A Unified Amber-Compatible Molecular Mechanics Force Field for Thiolate-Protected Gold Nanoclusters. *J. Chem. Theory Comput.* **2016**, *12*, 1342–1350.

[3] Caleman, C.; van Maaren, P.J.; Hong, M., Hub, J.S.; Costa, L.T.; van der Spoel, D. Force Field Benchmark of Organic Liquids: Density, Enthalpy of Vaporization, Heat Capacities, Surface Tension, Isothermal Compressibility, Volumetric Expansion Coefficient, and Dielectric Constant. *J. Chem. Theory Comput.* **2012**, *8*, 61–74.

[4] van der Spoel, D.; van Maaren, P.J.; Caleman, C. Gromacs Molecule & Liquid Database. *Bioinformatics* **2012**, *28*, 752–753.

[5] Kim, Y.; Machida, K. Vibrational Spectra, Normal Vibrations and Infrared Intensities of Six Isotopic Benzoic Acids. *Spectrochimica Acta Part A: Molecular Spectroscopy* **1986**, *42***,** 881–889.

[6] Tolstorozhev, G.B.; Belkov, M.V.; Skornyakov, I.V.; Bazyl, O.K.; Artyukhov, V.Y.; Mayer, G.V.; Shdyro, O.I.; Kuzokov, P.V.; Brinkevich, S.D.; Samovich, S.N. Infrared Spectroscopy of Hydrogen Bonds in Benzoic Acid Derivatives. *J. Appl. Spectr.* **2014**, *81***,** 109–117.

[7] Koivisto, J.; Chen, X.; Donnini, S.; Lahtinen, T.; Häkkinen, H.; Groenhof, G.; Pettersson, M. Acid–Base Properties and Surface Charge Distribution of the Water-Soluble Au102(pMBA)44 Nanocluster. *J. Phys. Chem. C* **2016**, *120***,** 10041–10050.

[8] Maçôas, E. M. S.; Lundell, J.; Pettersson, M.; Khriachtchev, L.; Fausto, R.; Räsänen. Vibrational Spectroscopy of cis- and trans-formic Acid in Solid Argon. *J. Mol. Spectr.* **2013**, *219***,** 70–80.

[9] Maçôas, E. M. S.; Khriachtchev, L.; Fausto, R.; Räsänen, M. Photochemistry and Vibrational Spectroscopy of the Trans and Cis Conformers of Acetic Acid in Solid Argon. *J. Phys. Chem. A* **2004**, *108***,** 3380–3389.

[10] Maçôas, E. M. S.; Khriachtchev, L.; Pettersson, M.; Fausto, R.; Räsänen, M. Internal Rotation in Propionic Acid: Near-Infrared-Induced Isomerization in Solid Argon. *J. Phys. Chem. A* **2005**, *109***,** 3617–3625.

[11] Amiri, S.; Reisenauer, H. P.; Schreiner, P. R. Electronic Effects on Atom Tunneling:

Conformational Isomerization of Monomeric Para-Substituted Benzoic Acid Derivatives. *J. Am. Chem. Soc.* **2010**, *132*, 15902–15904.

[12] Nieminen, J.; Räsänen, M.; Murto, J. Matrix Isolation and *ab initio* Studies of Oxalic Acid. *J. Phys. Chem.* **1992**, *96*, 5303–5308.

[13] Reva, I. D.; Stepanian, S. G.; Adamowicz, L.; Fausto, R. Combined FTIR Matrix Isolation and Ab Initio Studies of Pyruvic Acid: Proof for Existence of the Second Conformer. *J. Phys. Chem. A* **2001**, *105*, 4773–4780.

[14] Maçôas, E. M. S.; Fausto, R.; Lundell, J.; Pettersson, M.; Khriachtchev, L.; Räsänen. Conformational Analysis and Near-Infrared-Induced Rotamerization of Malonic Acid in an Argon Matrix. *J. Phys. Chem. A* **2000**, *104*, 11725–11732.

[15] Maçôas, E. M. S.; Khriachtchev, L.; Pettersson, M.; Lundell, J.; Fausto, R.; Räsänen. Infrared-Induced Conformational Interconversion in Carboxylic Acids Isolated in Low-Temperature Rare-Gas Matrices. *Vibr. Spectr.* **2004**, *34*, 73–82.